Available online at www.sciencedirect.com
ScienceDirect
International Journal of Thermal Sciences 46 (2007) 953–962
International Journal of Thermal Sciences
www.elsevier.com/locate/ijts

Flow pattern formation and the transition to chaos in a confined container heated locally from below

Hiroyoshi Koizumi *

Department of Mechanical Engineering & Intelligent Systems, The University of Electro-Communications, Chofu, Tokyo 182-8585, Japan

Received 4 October 2005; received in revised form 6 December 2006; accepted 6 December 2006

Available online 9 February 2007

Abstract

Experimental and numerical studies on the effects of the Grashof number Gr, and the container height H on the air flow pattern and the bifurcation process to chaos of the roll-cell pattern in a confined rectangular container heated locally from below are presented. The dimensionless container size $\frac{L}{D} : \frac{W}{D} : \frac{H}{D}$ is 7 : 3 : arbitrary value, where H is the height of the container and D is the width of the centrally heated bottom wall in the short sidewall direction. The flow pattern map which depends on Gr and H/D was obtained mainly by experimentation. Two-dimensional (2D) rolls with their axes parallel to the long sidewalls, in which fluid descending along both cooled long sidewalls is maintained in the same direction, are always produced above both adiabatic bottom walls next to the centrally heated bottom wall. In addition to these two rolls, four types of convective flow patterns above the centrally heated bottom wall are observed: one pair of steady 2D rolls with their axes parallel to the long sidewalls or a similar pair of steady 3D roll-cells in which cell structures exist within the rolls, unsteady 3D cells, and 3D oscillatory flow. For $Gr = 1.8 \times 10^6$ and $H/D = 0.20$, the 3D roll-cell pattern changes directly from time-dependent sinuous oscillatory motion to chaotic flow. Two positive Lyapunov exponents appear, and the Lyapunov dimension is about 3.7, indicating that this flow may be strongly chaotic. This non-cascade-type transition is due to the sudden flow pattern change from the single pair of the 3D roll-cell to the chaotic cell structure.

Keywords: Natural convection; Air flow; Flow pattern; Roll-cell structure; Transition; Chaos; Confined rectangular container; Locally heated bottom wall

1. Introduction

Recently, an idea has been proposed to submerge a large amount of CO_2, which is a major cause of global warming, into the deep sea [1,2]. This idea involves sherbet-like clustered CO_2 (liquid CO_2 is trapped within sherbet-like water under the conditions of low temperature and high pressure) being transported to the bottom of the deep sea by pipe line, and then pooled at the bottom of a ravine as shown in Fig. 1(a). The clustered CO_2 has a larger density than seawater of over 3000 m. It would be necessary to keep the clustered CO_2 for a long period of time in the deep sea, but there is concern that unsteady strong vortices around a transport pipe would enhance convective diffusion of the clustered CO_2 in the region near the pipe outlet. The flow and heat transfer performance around a cold horizontal cylinder placed near the bottom of the sea is shown schematically in Fig. 1(b-1) and can be roughly understood by the natural convective flow around a hot horizontal cylinder placed near a flat ceiling as shown in Fig. 1(b-2). These two flow systems are the approximate adverse flow phenomena which are caused by reversing both the vertical axis and temperature. The real interfacial boundary shown in Fig. 1(b-1) is a sherbet-like clustered CO_2, but the boundary of Fig. 1(b-2) is a liquid–solid wall.

A local electric power company in Japan has estimated the diameter of the actual transport pipe to be about 1 m and the average velocity in the pipe to be about 3 $\mathrm{m\,s^{-1}}$ in order to dispose the clustered CO_2 of 2.5 $\mathrm{ton\,s^{-1}}$ into the deep sea. The expected temperature difference between the seawater around the pipe and inside the pipe would be estimated to be within several degrees, but many unsolved problems remain in order to realize the successful disposal of clustered CO_2 in the deep sea [2].

The former experimental research of Ref. [3], which deals with a hot horizontal cylinder placed near a flat ceiling for air flow as shown in the upper part of Fig. 2, reveals that three

* Tel./fax: +81 42 443 5395.
E-mail address: koizumi@mce.uec.ac.jp.

1290-0729/$ – see front matter
doi:10.1016/j.ijthermalsci.2006.12.001

Nomenclature

D	width of the heated bottom wall in the short sidewall direction (Fig. 3), 76 mm
D_L	Lyapunov dimension
d_m	embedding dimension
Gr	Grashof number, $g\beta(T_{bh} - T_{tc})D^3/\nu^2$
H	height of the container which is able to be set an arbitrary value
L	length of the container, $7D = 532$ mm (length of the long sidewall)
$\frac{L}{D} : \frac{W}{D} : \frac{H}{D}$	dimensionless container size, 7 : 3 : arbitrary value
P	pressure
Pr	Prandtl number, ν/α
t	time
T	temperature
u, v, w	x, y, z components of the velocity
W	width of the container, $3D = 228$ mm (length of the short sidewall)
x, y, z	coordinates (Fig. 3), $x = y = z = 0$; bottom left-side corner of the container

Greek letters

α	thermal diffusivity
β	coefficient of thermal expansion
$\Delta\tau$	time interval of sampling
ΔT	temperature difference between the top cooled wall and the heated bottom wall, $T_{bh} - T_{tc}$
Θ	non-dimensional temperature, $(T - T_m)/(T_{bh} - T_{tc})$, where $T_m = (T_{bh} + T_{tc})/2$
λ_i	Lyapunov exponent ($i = 1, \ldots, d_m$)
ν	kinematic viscosity

Subscripts

bh	bottom, heated wall
ba	bottom, adiabatic wall
f	fluid
lw	long sidewall
m	mean temperature between the top cooled and bottom heated walls
sw	short sidewall
tc	top, cooled wall

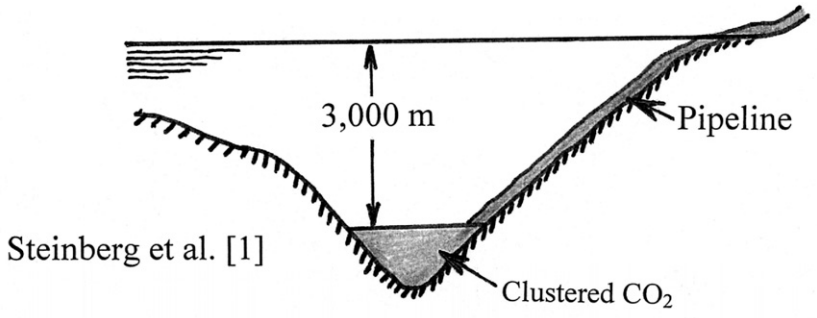

(a) Schematic drawing of the disposal of clustered CO_2 in the deep sea.

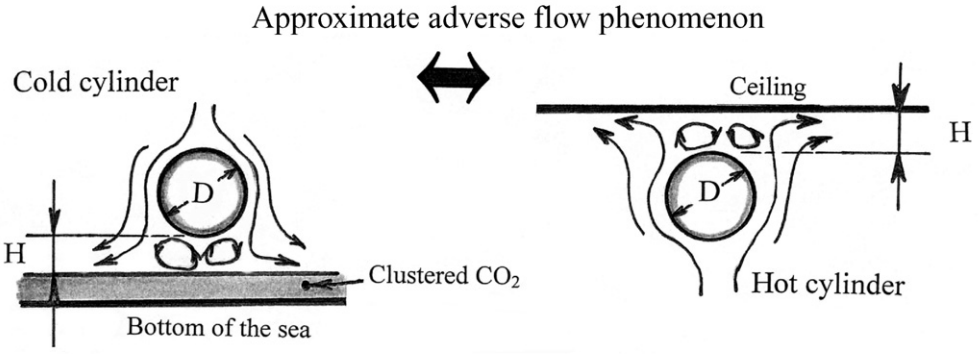

(b-1) Schematic flow pattern around the cold horizontal cylinder placed near the bottom of the sea.

(b-2) Schematic flow pattern around the hot horizontal cylinder placed near the flat ceiling.

Fig. 1. Proposal for the disposal of clustered CO_2 in the deep sea, and the concern of the diffusion problem of CO_2.

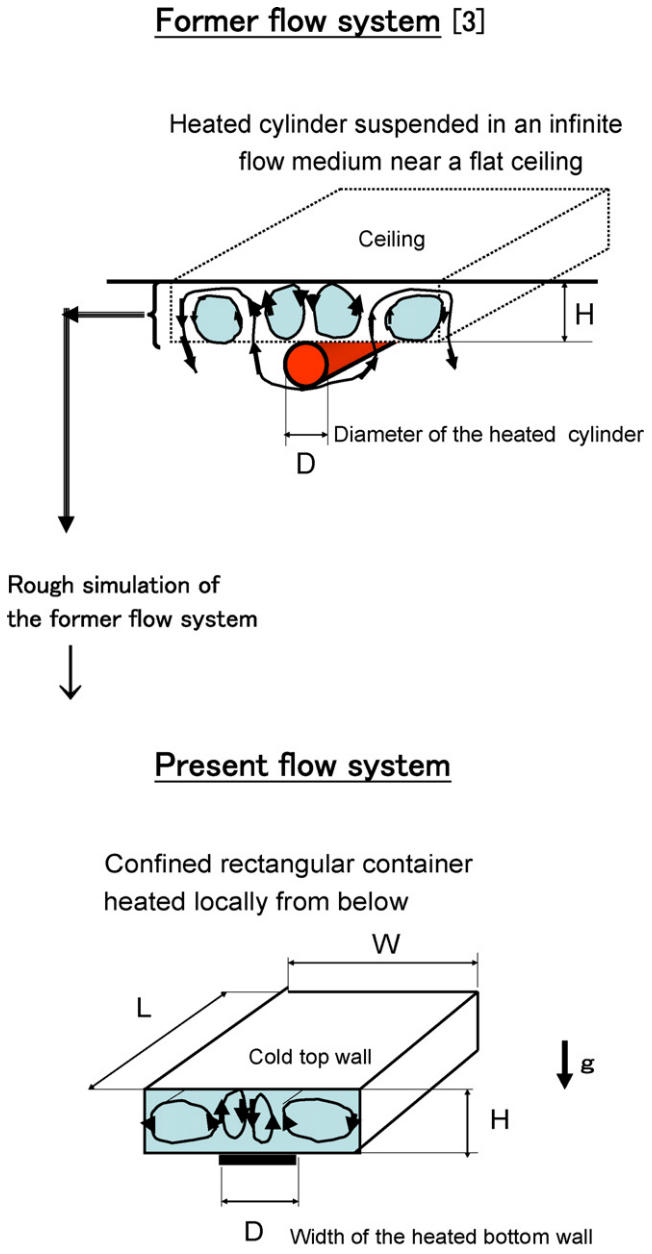

Fig. 2. Schematic drawing of the present flow system which roughly simulates the former flow system of a hot horizontal cylinder placed near a flat ceiling.

types of flow patterns are observed depending on the Grashof number Gr and the dimensionless distance H/D between the ceiling and the cylinder (D is the diameter of the heated cylinder in this flow system). These flow patterns are the 2D steady flow, low dimensional chaotic flow, and the 3D oscillatory flow. However, the effect of the Prandtl number Pr on the flow pattern and the bifurcation process to chaos could not be revealed. Furthermore, it is difficult to simulate the transition process to chaos around a hot horizontal cylinder placed near a flat ceiling in an infinite flow medium. In order to analyze the flow system precisely, for example, it is necessary to use the bipolar coordinate transformation. Then the circumference of a cylinder is converted into a line, and a fine grid near the cylinder and a coarse grid far from the cylinder could be set.

The aim of the present experimental and numerical study is to investigate the flow pattern formation and the transition process to chaos of roll-cells in terms of air flow ($Pr = 0.71$) in a confined rectangular container heated locally from below as shown in the lower part of Fig. 2, which roughly simulates the hot horizontal cylinder placed near a flat ceiling as shown in the upper part of Fig. 2. That is, this flow system focuses only on the narrow region between the heated cylinder and the ceiling which is enclosed by the dotted rectangular box as shown in the upper part of Fig. 2. It is thus expected that the transition process to chaos around the heated cylinder suspended in an infinite flow medium near a flat ceiling could be basically understood by analyzing the present flow system. Furthermore, to reveal the transition process of a roll-cell pattern to chaos in a large aspect ratio container such as the one used in this flow system, in which higher order chaotic flow may be produced, would be an interesting finding from the view point of basic heat transfer science.

Flow pattern formation is determined by non-linear aspects of the system under study, and also the Prandtl number Pr mainly governs the characteristics of non-linearity in the flow system. Therefore, the onset of the time dependence and the transition to chaos are especially strongly dependent on Pr [4,5].

Natural convective flow above horizontal heated surfaces appears in a wide variety of physical environments such as thermal plumes and geophysical phenomena. Therefore, a large number of Rayleigh–Bénard convections for both infinite layers and confined containers heated from below have been studied theoretically, experimentally and numerically. For example, Cross and Hohenberg [6] have extensively clarified the flow pattern formation and the transition process to chaos, both of which depend on Ra, Pr, and geometrical constraints.

On the contrary, only a few studies have examined flow pattern formation and heat transfer performance in a confined container heated locally from below. To reveal the change of flow and heat transfer performances affected by a wall of a confined container heated locally from below is important from the standpoint of industrial engineering in relation to the cooling of electronic devices. Sezai and Mohamad [7] numerically studied natural convection in air due to a discrete flush-mounted rectangular heat source on the bottom of a horizontal container. Aydin and Yang [8] simulated the steady natural convection heat transfer of air in a 2D square container with localized heating applied by a strip placed at the bottom center wall and by applying symmetric cooling from the side walls. Their analysis included the influence of the heated strip width and Rayleigh number on the fluid flow and heat transfer. Another similar industrial application, for example, is the melting of glass in which horizontal heated surfaces play a significant role in a rectangular open tank with a heated strip of width D at the bottom of the tank. Sarris et al. [9] investigated the effects of the Rayleigh number, the geometry of the heated strip and the tank on flow patterns and heat transfer by numerical simulation. Nevertheless, the transition process to chaos for horizontal containers heated locally from below has not been studied thus far.

2. Experimental methods and numerical simulation

2.1. Description of experiment

Fig. 3 shows a schematic drawing of the experimental apparatus and the coordinate system. The dimensions of the rectangular container are $L = 532$ mm (long sidewall), $W = 228$ mm (short sidewall), and the height H mm. The center part of one-third of the bottom wall in the short sidewall direction, of which width D is 76 mm and length L is 532 mm, was heated at constant temperature T_{bh}. The bottom heated wall was made of a 10 mm thick copper plate heated by a thin stainless steel foil, 30 μm thick, insulated from the copper plate. The foil was electrically heated by a constant direct current. The isothermal boundary condition of the copper surface was checked by measuring the surface temperature at several different positions by attaching a Cu–Co thermocouple of diameter 0.1 mm, and the surface temperature was kept uniform and constant within 0.2 K. Each one-third of the bottom wall next to the centrally heated bottom wall, which was made of foam glass, was adiabatic. The top wall and the four sidewalls were cooled at constant temperature T_{tc} by using a water reservoir made of 5 mm thick copper plate. The entire experimental setup consisted of two parts. One is the fixed cooled reservoir of top and four side walls, and the other is the locally heated bottom wall. The bottom wall was placed on the traversing system, and then the container height of H could be adjusted within the traversing precision of a 0.1 mm interval in the vertical direction.

The dimensionless container size $L/D : W/D : H/D$ is 7 : 3 : arbitrary value, and the height H/D was able to be set below 0.4. Experiments were carried out with air ($Pr = 0.71$) as the working medium at Grashof numbers ranging from 3.0×10^5 ($\Delta T \simeq 5$ K) to 1.8×10^6 ($\Delta T \simeq 30$ K). The Grashof number was set by changing the temperature difference, $\Delta T = T_{\mathrm{bh}} - T_{\mathrm{tc}}$, between the cooled top wall T_{tc} and the heated bottom wall T_{bh}. Physical properties were estimated at the mean temperature T_m.

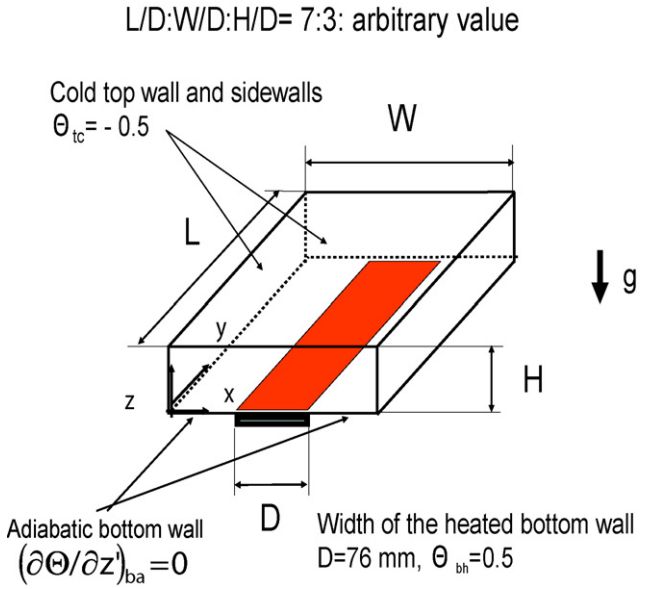

Fig. 3. Schematic drawing of the experimental apparatus and coordinate system.

In order to clarify the unsteady characteristics, an instantaneous flow visualization experiment was conducted using incense smoke. The sensor used to measure the air temperature was a thermocouple. The diameter of its copper and constantan wires was 50 μm, and the response time was approximately 0.2 s. This response time is sufficient to capture the chaotic behavior as shown in Figs. 7 and 8, because chaotic fluctuation frequencies are below about 0.5 Hz. The power spectrum was obtained using an FFT analyzer.

Phase trajectory and Lyapunov exponents λ_i ($i = 1, 2, \ldots, d_m$) were obtained using the time series of the temperature at the center part of the container by using a personal computer. The Lyapunov exponents λ_i represent the time-development of the displacement vector between two very adjacent points in the phase space. When one or more positive exponents are obtained, the flow may be characterized as chaotic with the magnitude of the exponents indicating the time scale for predictability. Also the Lyapunov dimension D_L, which shows the complexity of the attractor, was calculated from these exponents. The Lyapunov exponents could be calculated by the method proposed by Sano and Sawada [10].

The sampling time $\Delta\tau$ was set to 0.01953 s by using an analog to digital converter with 16 bit resolution. An attractor was reconstructed in a d_m-dimensional phase space by using 131 072 data points. Delay time τ_{del} is chosen as the lag time at which the autocorrelation function of the time series falls to nearly zero. Then the Lyapunov exponents λ_i was obtained from the orbits of points evolving in the time interval of τ_{dev}. A detailed description of the analyzing method is given in a previous published paper of Ref. [11]. The entire experimental apparatus was maintained at the same uniform and constant temperature within 1 K while each surface temperature was monitored during the entire acquisition time of 43 minutes (131 072 data × 0.01953 s).

2.2. Numerical modeling

The non-dimensionalized governing equations for unsteady 3D natural convection flow under the usual assumptions of a Boussinesq fluid, and negligible viscous dissipation and pressure work can be written in Cartesian coordinates as follows:

$$\frac{\partial u'}{\partial x'} + \frac{\partial v'}{\partial y'} + \frac{\partial w'}{\partial z'} = 0 \tag{1}$$

$$\frac{Du'}{Dt'} = -\frac{\partial P'}{\partial x} + Pr \cdot \nabla^2 u' \tag{2}$$

$$\frac{Dv'}{Dt'} = -\frac{\partial P'}{\partial y'} + Pr \cdot \nabla^2 v' \tag{3}$$

$$\frac{Dw'}{Dt'} = -\frac{\partial P'}{\partial z'} + Pr \cdot \nabla^2 w' + Gr \cdot Pr^2 \cdot \Theta \tag{4}$$

$$\frac{D\Theta}{Dt'} = \nabla^2 \Theta \tag{5}$$

with substantial derivative

$$\frac{D}{Dt'} = \frac{\partial}{\partial t'} + u' \frac{\partial}{\partial x'} + v' \frac{\partial}{\partial y'} + w' \frac{\partial}{\partial z'}$$

The x, y, and z coordinates were non-dimensionalized by D which is the width of the heated bottom wall in the short sidewall direction, the velocities were scaled by α/D, the time by D^2/α, and the pressure by $\rho\alpha^2/D^2$, respectively, where α is the thermal diffusivity, and ρ is the density of fluid. The dimensionless temperature was defined by $\Theta = (T - T_m)/(T_{bh} - T_{tc})$, where $T_m = (T_{bh} + T_{tc})/2$. Gr is the Grashof number, and Pr is the Prandtl number.

Approximate forms of the Boussinesq equations were obtained using a control volume method. The convective terms were discretized using a hybrid scheme (a first order accurate upwind difference scheme combined with second order central differencing). The SIMPLE algorithm [12] was used to solve these equations. In order to determine possible 3D effects, the entire enclosure was treated as the full computational domain. A grid system with uniform spacing, whose lattice point number was 35 (short sidewall in the x direction) $\times$ 53 (long sidewall in the y direction) $\times$13 (vertical sidewall in the z direction), was used for the coarser grid. A larger $53 \times 79 \times 19$ grid was employed for unsteady 3D cells at $Gr = 1.8 \times 10^6$ and $H/D = 0.204$ in region III of Fig. 4. Almost the same results were obtained for these two mesh sizes, and the calculated flow pattern was qualitatively in agreement with the experimental result as shown in Fig. 7(a-2). For these reasons, a $35 \times 53 \times 13$ uniform grid was selected for all calculations in the present study using a personal computer. It took over 20 hours of CPU time for the chaotic flow to be calculated as shown in Fig. 8 in the case of the $35 \times 53 \times 13$ grid system.

Boundary conditions were $u' = v' = w' = \frac{\partial P'}{\partial n'} = 0$ at all walls, and the wall temperature satisfied $\Theta_{bh} = 0.5$ at the heated bottom wall, $(\frac{\partial \Theta}{\partial z'})_{ba} = 0$ at the insulated bottom wall, and $\Theta_{tc} = \Theta_{sw} = \Theta_{lw} = -0.5$ at the top wall and sidewalls.

In order to clarify the effects of the sidewall temperature condition on the flow pattern, calculation was performed for the adiabatic sidewall condition at $Gr = 1.8 \times 10^6$ and $H/D = 0.200$ which corresponded to the results for constant temperature sidewall conditions shown in Fig. 5. Both calculated cell sizes within rolls were almost the same except only near the short sidewalls. Therefore, a constant and uniform sidewall temperature condition was used in this study to facilitate the comparison with experiments in which four sidewalls were cooled by using a water reservoir.

The initial conditions were those of a stagnant fluid with the temperature set to $\Theta_f = -0.5$. Convergence within each time step is determined through the sum of the absolute relative errors for each dependent variable in the entire flow field for all calculations:

$$\sum_{i,j} \frac{|\phi_{i,j}^{k+1} - \phi_{i,j}^{k}|}{|\phi_{i,j}^{k}|} \leqslant 10^{-5}$$

where, ϕ represents the variables u', v', w' or Θ, the superscript k refers to the iteration number and the subscripts i and j refer to the space coordinates. The dimensionless time step $\Delta t'$ was 0.0002 for the unsteady calculations. The time series of the temperature at the center grid point of the container were recorded and analyzed to obtain the phase trajectory and the power spectrum. All calculations were carried out with double precision.

Velocity vectors and isotherms in Figs. 5–8, grid lines of the velocity vectors and isotherms do not correspond to the number of grid lattices in the numerical simulation due to the used flow visualization program.

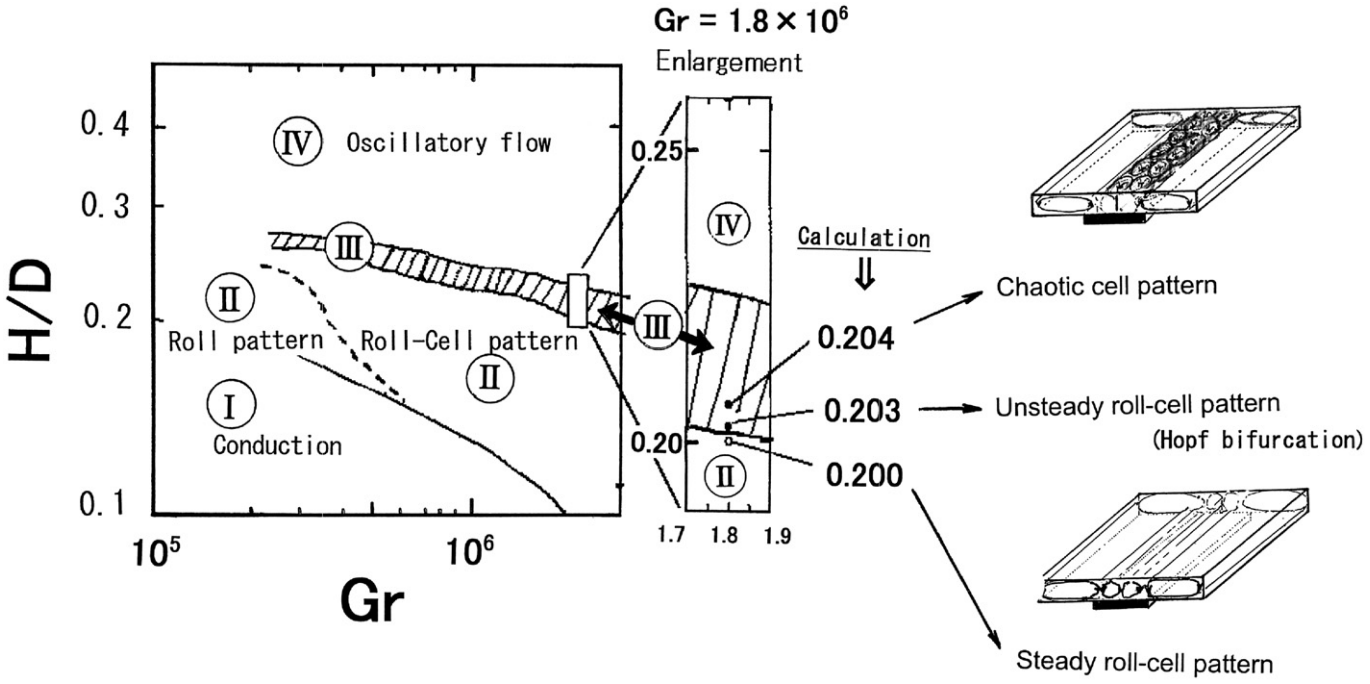

Fig. 4. Flow pattern map.

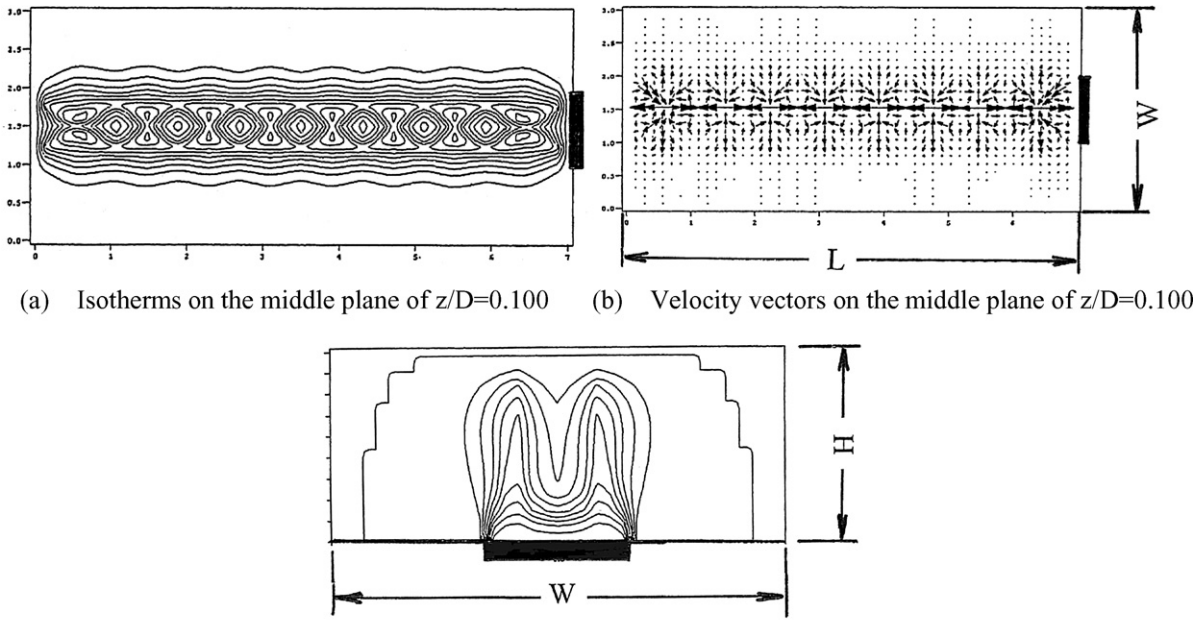

(a) Isotherms on the middle plane of z/D=0.100 (b) Velocity vectors on the middle plane of z/D=0.100

(c) Isotherms in the x-z cross-section at y/D=3.5

Fig. 5. Flow characteristics of a steady pair of roll-cells at $Gr = 1.8 \times 10^6$ and $H/D = 0.200$ in region II which was obtained by numerical simulation.

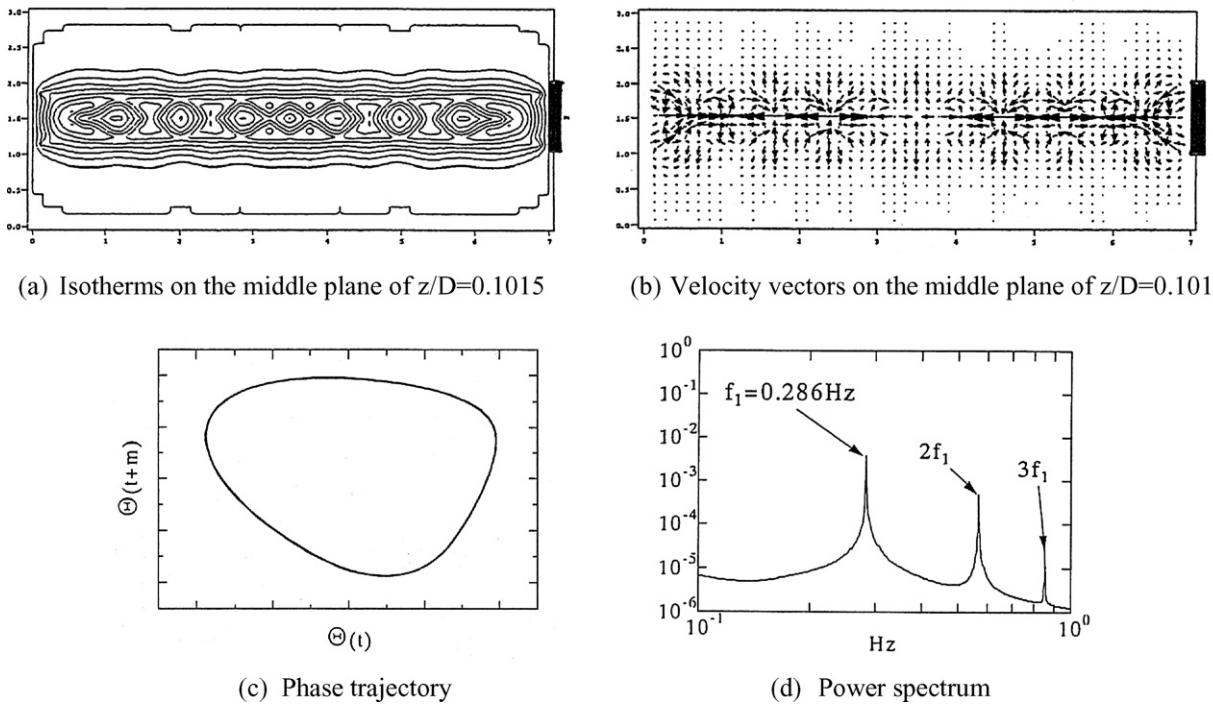

(a) Isotherms on the middle plane of z/D=0.1015 (b) Velocity vectors on the middle plane of z/D=0.1015

(c) Phase trajectory (d) Power spectrum

Fig. 6. Flow characteristics of the periodic 3D roll-cell pattern at $Gr = 1.8 \times 10^6$ and $H/D = 0.203$ which was obtained by numerical simulation.

3. Results and discussion

3.1. Flow pattern map

Fig. 4 shows the categorization of flow patterns and their dependence on the Grashof number Gr and the dimensionless container height H/D obtained mainly by experimentation.

2D rolls with their axes parallel to the long sidewalls, in which fluid descending along both cooled long sidewalls is maintained the same direction, are always produced above both adiabatic bottom walls next to the centrally heated bottom wall as shown in the schematic drawings of the flow pattern map in Fig. 4. In addition to these two large rolls, four types of convective flow patterns above the heated bottom wall are observed: one pair of steady 2D rolls with their axes parallel to the long sidewalls only for $Gr < 6 \times 10^5$ and $H/D < 0.25$ or a similar pair of 3D roll-cells in which cell structures exist within

Gr=1.8×10^6 and H/D=0.20

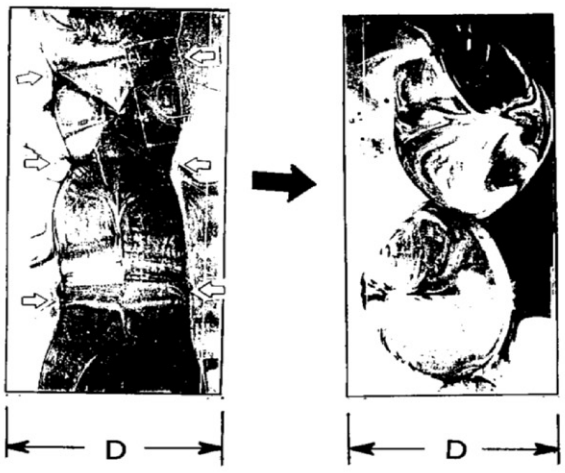

(a-1) (a-2)

Flow pattern above the heated bottom wall changes from photo (a-1) to photo (a-2) within a few seconds after the height was set to H/D= 0.20.

(a) Instantaneous flow visualization photos on the mid-plane of z/D=0.10.

	$d_m = 5$	$d_m = 6$	$d_m = 7$
λ_1	1.2 ±0.3	1.1 ±0.4	1.2 ±0.4
λ_2	0.3 ±0.1	0.3 ±0.2	0.3 ±0.2
λ_3	−0.5 ±0.1	−0.4 ±0.3	−0.4 ±0.2
λ_4	−1.6 ±0.4	−1.4 ±0.5	−1.5 ±0.4
λ_5	−4.5 ±0.9	−3.0 ±1.0	−2.5 ±1.0
λ_6		−6.9 ±2.1	−4.6 ±1.6
λ_7			−9.0 ±2.7
D_L	3.6 ±0.3	3.7 ±0.3	3.7 ±0.3

(b) Lyapunov exponents and their dimension.

Fig. 7. Chaotic flow characteristics at $Gr = 1.8 \times 10^6$ and $H/D = 0.20$ which was obtained by experimentation.

rolls, which is clearly shown in the flow visualization photo of Fig. 7(a-1), mainly for high Gr numbers and large H/D in region II, unsteady 3D cells in region III, and 3D oscillatory flow in region IV. The 3D oscillatory flow, which ascends from the central part of the heated bottom wall and descends along both long sidewalls, begins to oscillate extensively from side to side between top and bottom walls.

Fig. 5 shows the flow characteristics of a steady pair of roll-cells at $Gr = 1.8 \times 10^6$ and $H/D = 0.200$ in region II of Fig. 4 which was obtained by numerical simulation. Figs. 5(a) and (b) are the isotherms and velocity vectors on the mid-plane of $z/D = 0.100$, and Fig. 5(c) is the isotherms in the x–z cross-section at $y/D = 3.5$, but the container size ratios of length, width and height are not to scale. A steady roll-cell pattern with seven similar dimensional cells symmetrically aligned in series above the heated bottom wall is observed.

3.2. Transition to chaos of a steady 3D roll-cell pattern at $Gr = 1.8 \times 10^6$

The representative transition process to chaos from a single pair of a steady 3D roll-cell pattern in region II to an unsteady 3D cell pattern at $Gr = 1.8 \times 10^6$ in region III of Fig. 4 was investigated both numerically and experimentally. One pair of a steady 3D roll-cell patterns at $H/D = 0.200$ in the enlargement of region II of Fig. 4 begins to exhibit time-dependent periodic flow at $H/D = 0.203$, and then a successive bifurcation occurs from the periodic flow directly into the

3D chaotic cell flow at $H/D = 0.204$ in region III by numerical simulation. Fig. 6 shows the time-dependent periodic flow characteristics at $H/D = 0.203$. Figs. 6(a) and (b) are the instantaneous isotherms and velocity vectors on the mid-plane of $z/D = 0.1015$. Fig. 6(c) is the phase trajectory, and Fig. 6(d) is the power spectrum, respectively.

This unsteady 3D roll-cell pattern was changed from the steady 3D roll-cell pattern with seven same dimensional cells symmetrically aligned in series above the heated bottom wall as shown in Fig. 5. These unsteady seven cells were notably different in size from the steady seven cells as shown in Fig. 5(a). The roll-cell begins to oscillate with a spectral peak frequency of $f_1 = 0.286$ Hz, and the relative temperature fluctuation intensity ($\sqrt{(T_f - \bar{T}_f)^2}/\bar{T}_f$; T_f is the instantaneous fluid temperature, and $\bar{T}_f$ is the local time-averaged fluid temperature) which is about 1%. From the results of the time series analysis, Hopf bifurcation occurs clearly at $H/D = 0.203$.

Fig. 7 shows chaotic flow characteristics of 3D cells at $Gr = 1.8 \times 10^6$ and $H/D = 0.20$ in region III of Fig. 4 which was obtained by experimentation. These results correspond to the unsteady 3D cells at $H/D = 0.204$ just after the transition to chaos obtained numerically and are shown in Fig. 8.

Fig. 7(a) shows instantaneous flow visualization photos on the mid-plane of $z/D = 0.10$ above the heated bottom wall. Photos are shown only in the center part of the total heated bottom wall, which corresponds to the area of D (width of the heated bottom wall) × 2D (length along the long sidewall). One pair of 3D sinuous oscillatory roll-cells (cell structures exist within the roll) with several necked parts is shown by several arrows in Fig. 7(a-1), and this pair changes to unsteady 3D cell structures as shown in Fig. 7(a-2) within a few seconds after the height was set to 0.20. Each cell size is almost the same as the width of the heated bottom wall D and is aligned in a zigzag pattern along the heated bottom wall.

Fig. 7(b) is the Lyapunov exponents λ_i and Lyapunov dimension D_L, when the embedding dimension increases from $d_m = 5$ to $d_m = 7$. The sign ± in the Lyapunov exponents λ_i is calculated from several runs with different parameters τ_{dev}, ε_r, N within the following ranges. The developing time is $3\Delta\tau \leqq \tau_{\text{dev}} \leqq 6\Delta\tau$ for sampling time $\Delta\tau = 0.01953$ s. When the extent of the phase space is normalized as unity, the radius of a small ball is $0.03 \leqq \varepsilon_r \leqq 0.06$, and the number of the phase points included in it is $10 \leqq N \leqq 30$. Two positive Lyapunov exponents appear and D_L is about 3.7, therefore, this flow may be strongly chaotic. This non-cascade-type transition is due to the sudden flow pattern change from one pair of 3D sinuous oscillatory roll-cells, in which cell structures exist within rolls shown by the flow visualization photo of Fig. 7(a-1), to unsteady 3D cells of Fig. 7(a-2).

Flow pattern formation and time dependence in non-equilibrium dissipative systems such as convection in a horizontal fluid layer heated from below are problems of considerable interest, both from a practical point of view and as unresolved problems in physics. The dependence of pattern selection and time dependence on the shape and dimension of the container (i.e. the aspect ratios) and on the Rayleigh and Prandtl numbers have been systematically investigated for small containers. Changes in the flow pattern are severely restricted by the boundaries, and the flow becomes time dependent in a manner which is similar to that observed in dynamical systems of low dimensionality [5].

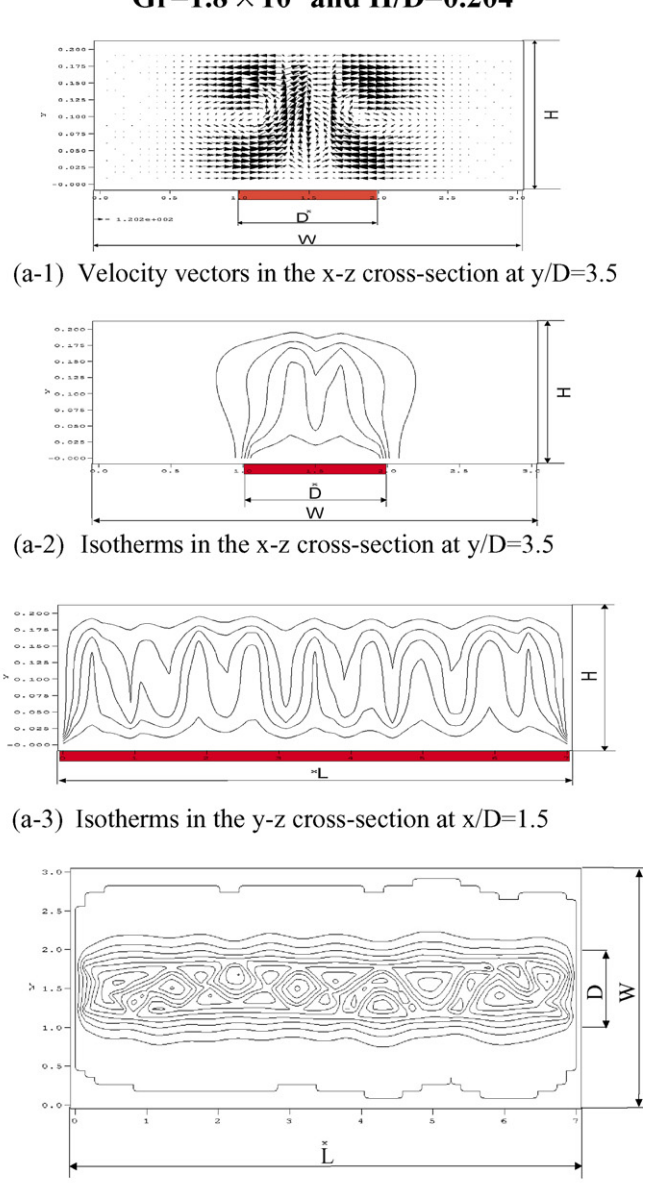

Fig. 8. Chaotic flow characteristics at $Gr = 1.8 \times 10^6$ and $H/D = 0.204$ which was obtained by numerical simulation.

On the other hand, spatially extended dynamical systems such as large containers and infinite fluid layers exhibit complex transitional behavior. The stability of parallel-roll convection was demonstrated as a function of Rayleigh number and roll wavenumber for various Prandtl numbers in a laterally infinite fluid layer, and the strong dependence of the instabilities on Pr was based on the result of the linearized analysis [4]. Furthermore, for large containers such as those used in this flow system, the initial time dependence of the roll pattern on the

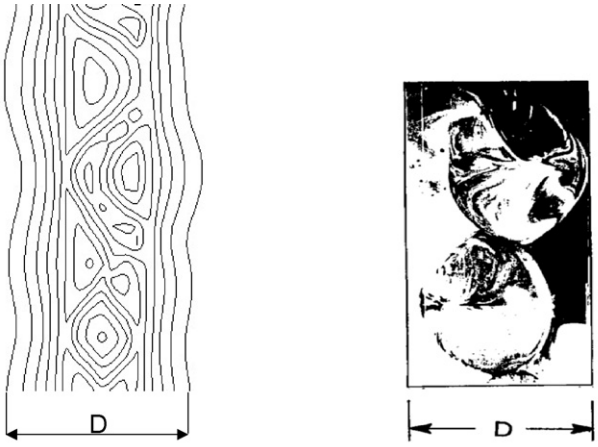

H/D=0.204 Isotherms

H/D=0.20 Flow visualization photo

(a-5) Comparison of 3-D cell-pattern between calculation and flow visualization on the mid-plane of H/D=0.102 above the heated bottom wall.

(a) Instantaneous velocity vectors and isotherms at various cross-sections.

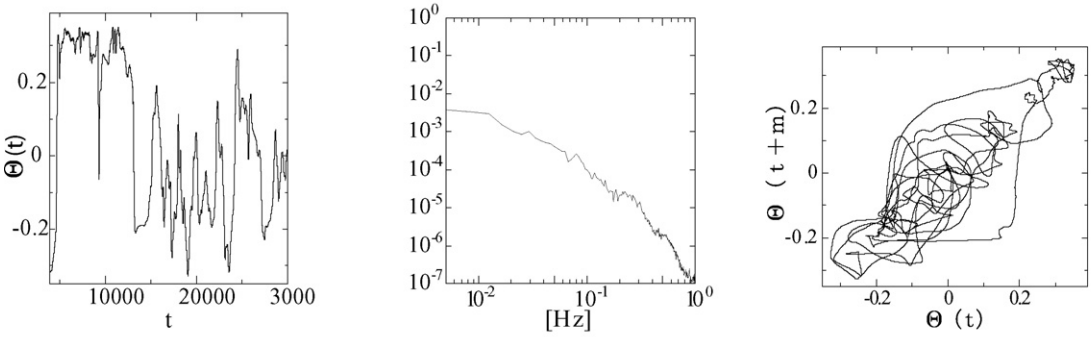

(b-1) Time series and its power spectrum.

(b-2) Phase trajectory

(b) Flow characteristics.

Fig. 8. (*continued*)

timescale of the horizontal-diffusion time is typically in slow motion, which is opposite that of the vertical-diffusion time is in rapid motion [13]. This slow motion makes it difficult to distinguish clearly other changes and instabilities in the pattern. Therefore, if the onset of chaotic time dependence could be observed, it would be difficult to judge whether the time dependent flow is a chaotic or a transient flow to another spatial flow pattern. Analysis of dynamical quantities such as Lyapunov dimensions and exponents plays an important role in judging the existence of chaotic attractor and its complexity. The Lyapunov dimension of the chaotic cell structure is 3.7 in the present flow system, and therefore this chaotic flow may be judged to be independent of a transient flow of roll-cell structure to another spatial flow pattern.

When a container is sufficiently large for one to observe changes in the spatial flow pattern well before the onset of chaotic time dependence, complex behavior in both space and time was observed [14]. But this flow system is clearly different from the spatiotemporal chaos, because the spatial flow pattern before the transition to chaotic flow as shown in Fig. 5 is very regular.

Fig. 8 shows calculated chaotic flow characteristics at $Gr = 1.8 \times 10^6$ and $H/D = 0.204$ in region III of Fig. 4, which correspond to the experimental characteristics just before the transition to chaos at $H/D = 0.20$ as shown in Fig. 7. Fig. 8(a) shows instantaneous velocity vectors and isotherms at various cross-sections, but the container size ratios of length, width and height are not to scale. Fig. 8(b) shows the flow characteristics.

Figs. 8(a-1) and (a-2) show the velocity vectors and isotherms in the x–z cross-section at $y/D = 3.5$. Fig. 8(a-3) shows the isotherms in the y–z cross-section at $x/D = 1.5$, and Fig. 8(a-4) shows the isotherms on the mid-plane of $z/D = 0.102$, respectively. Fig. 8(a-5) reveals the comparison of 3D cells between the calculated result in the region between $2.5 < y/D < 5.5$ and $1.0 < x/D < 2.0$ above the heated bot-

tom wall and the corresponding flow visualization photo of Fig. 7(a-2).

From the velocity vectors of Fig. 8(a-1) and isotherms of Figs. 8(a-2), (a-3) and (a-4), several numbers of large 3D cells, which descend in the center and ascend around the outer part of each cell are formed, these cells are aligned in a zigzag pattern with smaller cells between them along the center part of the long heated bottom wall. In addition to these cells, large 2D rolls with their axes parallel to the long sidewalls, which differ in their circulation direction above both adiabatic bottom walls, are produced. When the instantaneous flow visualization photo on the mid-plane of $z/D = 0.10$ on the right-side of Fig. 8(a-5) is compared to the isotherms obtained numerically at $H/D = 0.102$ on the left-side of Fig. 8(a-5), almost the same cell-pattern was obtained, but the simulated cell size is smaller than that of the experimental observation. The difference between these two cell sizes is due to the lack of spatial resolution in the numerical simulation. However, these numerical results have qualitatively elucidated the nature of the bifurcation process to chaos observed in the experimentation as shown in Fig. 7(a). Fig. 8(b-1) shows the time series of fluid temperature and its power spectrum, and Fig. 8(b-2) shows the phase trajectory. A considerable number of modes may be relevant in the transition due to the fact that the power spectrum is continuous and below about 0.5 Hz, and the trajectory in the phase space follows very complicated orbits.

4. Conclusion

Results have been presented of experimental and numerical studies concerning the transition from a roll-cell pattern to chaotic flow in a confined rectangular container heated locally from below. Experiments were performed with air ($Pr = 0.71$) at Grashof numbers ranging from 3.0×10^5 to 1.8×10^6. The representative length scale is defined by width D of the locally heated bottom wall in the short sidewall direction.

- The flow pattern and the transition process to chaos of certain buoyant container-flow problems heated locally from the bottom wall are significantly influenced by the thermal boundary conditions of the bottom wall.
- Four types of flow patterns above the locally heated bottom wall are observed for air flow depending on Grashof number Gr and dimensionless container height H/D between the cooled top wall and the locally heated bottom wall. These patterns consist of one pair of steady 2D rolls with their axes parallel to the long sidewalls or a similar pair of 3D roll-cells in which cell structures exist within rolls, unsteady 3D cells, and 3D oscillatory flow.
- The 3D roll-cell pattern changes directly from time-dependent periodic motion to chaotic flow at $Gr = 1.8 \times 10^6$ and $H/D = 0.20$ experimentally. This non-cascade-type transition is due to the sudden flow pattern change from sinuous oscillatory 3D roll-cells to chaotic 3D cells. Two positive Lyapunov exponents appear, and the Lyapunov dimension is about 3.7. These transitional characteristics to chaotic flow are qualitatively obtained by numerical simulation at $H/D = 0.204$.

Acknowledgements

The author is grateful to the graduated and undergraduate students at the University of Electro-Communications for their experimental and numerical performances throughout this work, and is indebted to the reviewers of this manuscript for their constructive suggestions that have influenced its quality.

References

[1] M. Steinberg, H.C. Cheng, F. Horn, A system study for the removal, recovery and disposal of carbon dioxide from fossil fuel power plants in the US, Report of Brookhaven National Laboratory, RNL-35666, 1984.
[2] H. Ishitani, R. Matsuhashi, S. Oomura, S. Shimada, T. Suyari, Feasibility study on CO_2 disposal in the ocean, Energy Resources 12 (1991) 296–304 (in Japanese).
[3] H. Koizumi, I. Hosokawa, Chaotic behavior and heat transfer performance of the natural convection around a hot horizontal cylinder affected by a flat ceiling, Int. J. Heat Mass Transfer 39 (1996) 1081–1091.
[4] F.H. Busse, Non-linear properties of thermal convection, Reports on Progress in Physics 41 (1978) 1929–1967.
[5] J.P. Gollub, S.V. Benson, Many routes to turbulent convection, J. Fluid Mech. 100 (1980) 449–470.
[6] M.C. Cross, P.C. Hohenberg, Pattern formation outside of equilibrium, Reviews of Modern Physics 65 (1993) 851–1086.
[7] I. Sezai, A.A. Mohamad, Natural convection from a discrete heat source on the bottom wall of a horizontal enclosure, Int. J. Heat Mass Transfer 43 (2000) 2257–2266.
[8] O. Aydin, W.J. Yang, Natural convection in enclosures with localized heating from below and symmetrical cooling from sides, Int. J. Numer. Mech. Heat Fluid Flow 10 (2000) 518–529.
[9] I.E. Sarris, I. Lekakis, N.S. Vlachos, Natural convection in rectangular tanks heated locally from below, Int. J. Heat Mass Transfer 47 (2004) 3549–3563.
[10] M. Sano, Y. Sawada, Measurement of the Lyapunov spectrum from a chaotic time series, Phys. Rev. Lett. 55 (1985) 1082–1085.
[11] H. Koizumi, I. Hosokawa, Unsteady behavior and mass transfer performance of the combined convective flow in a horizontal rectangular duct heated from below, Int. J. Heat Mass Transfer 36 (1993) 3937–3947.
[12] S.V. Patankar, Numerical Heat and Fluid Flow, Hemisphere, Washington, DC, 1980.
[13] J.P. Gollub, A.R. McCarriar, J.F. Steinman, Convective pattern evolution and secondary instabilities, J. Fluid Mech. 125 (1982) 259–281.
[14] D.A. Egolf, I.V. Melnikov, W. Pesch, R.E. Ecke, Mechanism of extensive spatiotemporal chaos in Rayleigh–Bénard convection, Nature 404 (2000) 733–736.